Computer Networks 225 (2023) 109663

Contents lists available at ScienceDirect

Computer Networks

journal homepage: www.elsevier.com/locate/comnet

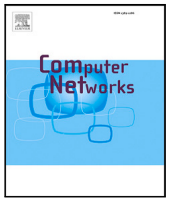

Experimental analysis of RSSI-based localization algorithms with NLOS pre-mitigation for IoT applications

Fabrizio Carpi [a,1], Marco Martalò [b,*,1], Luca Davoli [c], Antonio Cilfone [d,1], Yingjie Yu [e], Yi Wang [e], Gianluigi Ferrari [c]

[a] New York University (NYU), NY, USA
[b] Networks for Humans (Net4U) Laboratory, Department of Electrical and Electronic Engineering, University of Cagliari, and CNIT, Cagliari, Italy
[c] Internet of Things (IoT) Laboratory, Department of Engineering and Architecture, University of Parma, CNIT, and CINI, Parma, Italy
[d] Tesmec Automation s.r.l., Fidenza, Italy
[e] Huawei Technologies Co. Ltd., Shanghai, China

ARTICLE INFO

Keywords:
Internet of Things (IoT)
Line-Of-Sight (LOS)
Non-LOS (NLOS)
Channel status identification
IEEE 802.11
LTE
NLOS mitigation
Positioning

ABSTRACT

In this paper, we propose an effective target localization strategy for Internet of Things (IoT) scenarios, where positioning is performed by resource-constrained devices. Target-anchor links may be impaired by Non-Line-Of-Sight (NLOS) communication conditions. In order to derive a feasible IoT-oriented positioning strategy, we rely on the acquisition, at the target, of a sequence of consecutive measurements of the Received Signal Strength Indicator (RSSI) of the wireless signals transmitted by the anchors. We then consider a pragmatic approach according to which the NLOS channels are pre-mitigated and "transformed" into equivalent Line-Of-Sight (LOS) channels to estimate more accurately each target-anchor distance. The estimated distances feed "agnostic" localization algorithms, operating as if all links were LOS. We experimentally assess the performance of our approach in indoor (IEEE 802.11-based) and outdoor (Long Term Evolution, LTE-based) scenarios, considering both geometric and Particle Swarm Optimization (PSO)-based localization algorithms. Even if NLOS mitigation per single communication link is very effective, our results show that, in a given environment, it is possible to derive an "average" NLOS mitigation strategy regardless of the specific position of the target in the given environment. This is crucial to limit the computational complexity at IoT nodes performing localization, yet guaranteeing a relatively high (for IoT scenarios) localization accuracy, especially in an IEEE 802.11-based indoor case (with six anchors). The obtained performance compares favorably (in relative terms) with that obtained with more sophisticated wireless technologies (e.g., Ultra-WideBand, UWB).

1. Introduction

User localization is a crucial requirement for modern networks (e.g., cellular networks), since it allows providers to offer enhanced location-based services [1]. The Internet of Things (IoT) will also benefit from these services, as adding location information may limit the need for human intervention [2].

Radio-based positioning relies on distance estimates between the target and a few reference (with known positions) nodes, denoted as *anchors*. Such estimates can be obtained from relevant parameters, depending on the considered radio technology, such as: Received Signal Strength Indicator (RSSI), Angle of Arrival (AoA), Time of Arrival (ToA), Time Difference of Arrival (TDoA) [3]. In [4], an enhanced fingerprinting method is considered, by relying on crowdsourced data kept from smartphones. In [5], a few positioning techniques are analyzed considering various experimental IoT wireless technologies: Zigbee, Bluetooth Low Energy (BLE), and WiFi (2.4 GHz band). In [6], AoA fingerprinting is improved by leveraging the available Channel State Information (CSI). In [7], RSSI-based localization is improved by means of Machine Learning (ML)-based techniques and, in particular, using Deep Reinforcement Learning (DRL).

User and device localization has been already exploited in IoT-based applications by leveraging various technologies. In the presence of large networking scenarios, the number of acquired RSSI data may explode. In order to reduce the amount of acquired RSSI data, in [8] a compression method is proposed. Low-complexity data processing for positioning in resource-constrained devices is also addressed in [9]. In [10],

* Corresponding author.
E-mail addresses: fabrizio.carpi@nyu.edu (F. Carpi), marco.martalo@unica.it (M. Martalò), luca.davoli@unipr.it (L. Davoli), antonio.cilfone@tesmec.com (A. Cilfone), yuyingjie1@huawei.com (Y. Yu), yi.wang@huawei.com (Y. Wang), gianluigi.ferrari@unipr.it (G. Ferrari).
[1] F. Carpi, M. Martalò, and A. Cilfone were with the IoT Lab of the University of Parma when contributing to this work.

https://doi.org/10.1016/j.comnet.2023.109663
Received 18 January 2022; Received in revised form 27 October 2022; Accepted 25 February 2023
Available online 2 March 2023

low-complexity RSSI-based localization in WiFi networks is proposed. In [11], visible light communications are considered to achieve a centimeter level accuracy. Range-free methods can also be considered to limit the complexity of the localization system, as shown in [12].

Radio-based positioning algorithms are impaired by physical obstructions and interference present in the surrounding environment, especially in indoor scenarios. In particular, in the presence of Line-Of-Sight (LOS) communications between the target and the anchors, the reliability of the position estimate may be very high. On the other hand, in the presence of Non-Line-Of-Sight (NLOS) links, the reliability of the position estimate may drastically reduce [13]. Therefore, the problem of channel status (i.e., LOS/NLOS) identification is crucial in radio-based localization—see, for example, [14] and references therein. In [15,16], the LOS/NLOS classification problem is tackled, from an experimental point of view, in indoor IEEE 802.11-based scenarios. In [16], the authors propose a Deep Learning (DL)-based method in which RSSI and CSI data are jointly used for classification. In [17], DL is used for LOS/NLOS link classification in Ultra-WideBand (UWB) scenarios. In [15], we have proposed channel status identification based on thresholding of simple RSSI statistical features. The use of thresholding on simple RSSI statistical features for LOS/NLOS identification purposes is also considered in Radio Frequency IDentification (RFID) schemes. For instance, in [18] the authors propose a threshold-based method on the variance of RSSI and received phase values.

In general, the performance of a localization strategy can be improved by properly taking into account the presence of NLOS links. In [19], the authors discuss NLOS identification and mitigation in UWB scenarios: channel identification and mitigation algorithms are based on ML techniques fed by fine-grained features extracted from the received waveform (e.g., received energy, maximum amplitude, rise time, etc.) and acquired with extensive experimental measurement campaigns. A similar scheme is proposed in [20]. In [21,22], NLOS mitigation schemes are proposed under the assumption of a constant bias in the estimated target-anchor distances. In particular, novel location estimators are designed and validated in realistic UWB-based setups. Similarly, in [23] a position estimator is derived using optimization techniques and is validated using UWB communications. In [24], the authors propose identification and mitigation in indoor WiFi scenarios, by relying on fine-grained CSI at the physical layer. In [25], a UWB identification and mitigation approach based on a Convolutional Neural Network (CNN) architecture is proposed. This method leverages the availability of the Channel Impulse Response (CIR), which obviously provides more information on the channel status than the RSSI does. However, the use of RSSI is attractive in IoT scenarios with constrained nodes (with limited processing capabilities).

In this paper, we consider a static localization scenario, where positioning is performed by static (resource-constrained) IoT devices. In order to keep the computational complexity limited and derive a feasible approach, we simply rely on the use of RSSI measurements instead of more powerful ToA/TDoA processing strategies, which are not feasible in IoT scenarios (e.g., because of stringent synchronization requirements). RSSI values can be easily obtained with Commercial Off-The-Shelf (COTS) devices and we focus on IEEE 802.11 (WiFi) and Long Term Evolution (LTE) technologies (easily integrable). It is known that RSSI in NLOS links can be characterized by statistical features, such as skewness, kurtosis, and others—see, e.g., [15,16]. We leverage the identification method proposed in [15] to define and implement a NLOS mitigation scheme for enhanced localization. In particular, we use the feature-based classifier in [15] is a first processing stage to detect the presence of NLOS communication links; then, we exploit a linear combination of the same features to mitigate NLOS-induced ranging errors. Finally, after NLOS measurements are "corrected", a localization algorithm is applied to estimate the target position.

Unlike previous literature works which propose advanced signal processing strategies to incorporate NLOS mitigation (with complexity which may not be compatible with the constraints imposed by IoT devices), we aim at showing the effectiveness of a heuristic (yet reasonable) global NLOS mitigation method in an experimental environment. In particular, our proposed localization approach involves the following two steps.

- The *first* pre-processing step consists of the extraction, by the target node, of five statistical features from N (whose value is properly chosen) consecutive RSSI measurements from each link between the target and an anchor. These features are then compared to pre-determined thresholds to classify the status (LOS/NLOS) of the link [15]. In an initial "training phase", once a sufficiently large number of features have been collected over representative links in the environment where target will be placed, features' regression is considered to derive a unique average correction parameter to be applied to any NLOS link. This correction aims at mitigating the link distance error induced by NLOS effects and, thus, at "transforming" NLOS links into equivalent LOS ones.
  Our approach differs from those proposed in other literature works (see, e.g., [26,27]), in which mitigation is achieved by means of more sophisticated algorithms requiring an *a-priori* statistical characterization of LOS/NLOS channel status. The use of a common correction parameter, representative of the average NLOS conditions of the environment where the target is placed, is expedient to reduce the required complexity since no parameter retraining is needed if the target remains in the same environment. On the other hand, one may optimize the NLOS mitigation parameter for each target-anchor communication link to achieve a higher localization accuracy. However, this comes at the price of a higher computational complexity, which may be critical for IoT-oriented applications.
- In the *second* step, all estimated link distances are input to an "agnostic" localization algorithm, which operates as if all links were in LOS conditions. In other words, unlike previous works aiming at designing novel localization algorithms embedding NLOS mitigation, we investigate the direct applicability of existing localization algorithms after the proposed NLOS link pre-processing stage. This approach (together with RSSI-based processing) further keeps the overall computational complexity limited.

An experimental IoT-oriented performance analysis of the proposed localization strategies is carried out in both indoor (IEEE 802.11) and outdoor (LTE) scenarios.[2] Our results show that, in the best cases, the positioning error with average NLOS mitigation (i.e., using the same correction parameter for all links) is around (approximately) 30% and 60% of the maximum target-anchor distance in indoor and outdoor scenarios, respectively. The obtained performance is worse than, yet aligned with, that of more powerful communication technologies such as UWB, which, however, is not always suitable for IoT scenarios. In particular, in indoor scenarios, our results show that, with probability equal to 80%, the error with UWB is around 12% of the average target-anchor distance, whereas with WiFi is around 37%. Finally, if per-link optimized NLOS mitigation is applied (i.e., considering a specific correction parameter per link), this error can be significantly reduced, with a reduction up to 90% in outdoor scenarios and over 80% in indoor scenarios. As mentioned above, this comes at the price of a much higher computational complexity.

The rest of the paper is organized as follows. In Section 2, we introduce the system model. In Section 3, the proposed localization method with NLOS identification/mitigation is presented. Experimental results for IoT-oriented IEEE 802.11 and LTE systems are discussed in Section 4. Finally, concluding remarks are given in Section 5.

[2] For LTE-based analysis, we rely on the use of a smartphone. However, the obtained results are also meaningful for 4G NarrowBand-IoT (NB-IoT) scenarios, as the same RSSI values can be exploited.

2. System model

Let us consider a wireless scenario, in which a static[3] target node, at coordinates $\boldsymbol{u} = [x, y]^T$, receives packets from M transmitters, either Access Points (APs) or Base Transceiver Stations (BTSs), acting as anchors. The known position of the ith anchor is denoted as $\boldsymbol{s}_i = [x_i, y_i]^T$, $i \in \{1, \dots, M\}$, where $[\cdot]^T$ is the transpose operator. The set of anchor nodes' coordinates can be organized in the following matrix:

$$\boldsymbol{S} = \begin{bmatrix} x_1 & x_2 & \dots & x_M \\ y_1 & y_2 & \dots & y_M \end{bmatrix} = \left[\boldsymbol{s}_1, \dots, \boldsymbol{s}_M\right]. \tag{1}$$

This scenario is meaningful for applications in which targets (people and/or objects) to be localized are moving on the x–y plane, e.g., IoT tags moving on a given building floor. The extension to a three-dimensional case is straightforward, but goes beyond the scope of this paper.

The goal of a localization system is to derive an estimate of the target node's position, denoted[4] as $\hat{\boldsymbol{u}} = [\hat{x}, \hat{y}]^T$, given $\boldsymbol{S}$ and a set of measurements of the target-anchor links. The Euclidean norm of the ith anchor's coordinates, i.e., the distance of that anchor from the axes' origin, is defined as

$$k_i = \|\boldsymbol{s}_i\| = \sqrt{\boldsymbol{s}_i^T \boldsymbol{s}_i} \qquad i = 1, \dots, M.$$

The anchors' norm vector is then $\boldsymbol{k} = [k_1, \dots, k_M]^T$.

Let $\boldsymbol{d} = [d_1, d_2, \dots, d_M]^T$ be the vector containing the (true) link distances between the target node and the M anchors, where the ith distance can be written as

$$d_i = \|\boldsymbol{u} - \boldsymbol{s}_i\| = \sqrt{(\boldsymbol{u} - \boldsymbol{s}_i)^T(\boldsymbol{u} - \boldsymbol{s}_i)} \quad i = 1, \dots, M. \tag{2}$$

Let $\hat{\boldsymbol{d}}$ denote the corresponding vector of distance estimates, in which the ith term can be written as

$$\hat{d}_i = \|\hat{\boldsymbol{u}} - \boldsymbol{s}_i\| = \sqrt{(\hat{\boldsymbol{u}} - \boldsymbol{s}_i)^T(\hat{\boldsymbol{u}} - \boldsymbol{s}_i)} \quad i = 1, \dots, M. \tag{3}$$

For instance, $\hat{d}_i$ is the ith link distance estimate computed from the acquired data (e.g., RSSIs).

The localization problem can be generally modeled as the following system of equations containing anchors' positions and range estimates:

$$\begin{cases} (\hat{x} - x_1)^2 + (\hat{y} - y_1)^2 = \hat{d}_1^2 \\ \qquad\qquad \vdots \\ (\hat{x} - x_M)^2 + (\hat{y} - y_M)^2 = \hat{d}_M^2. \end{cases} \tag{4}$$

In order to solve this system of equations in the unknowns $[\hat{x}, \hat{y}]$, different solutions will be proposed in Section 3.4.

While ToA-based localization algorithms work on the basis of estimated distances $\{\hat{d}_i\}$, TDoA-based algorithms rely on relative distance estimates with respect to a reference anchor. Assuming, for notational simplicity, that $\boldsymbol{s}_1$ is the anchor with the shortest estimated distance, then the vector of relative distances (with respect to $\boldsymbol{s}_1$) is defined as $\boldsymbol{\Delta} = [\Delta_1, \dots, \Delta_M]^T$, in which the ith term is

$$\Delta_i = d_i - d_1 \tag{5}$$

and its estimate is

$$\hat{\Delta}_i = \hat{d}_i - \hat{d}_1. \tag{6}$$

Note that $\Delta_1 = \hat{\Delta}_1 = 0$ by construction. The quantities $\{\hat{\Delta}_i\}_{i=1}^M$ can be interpreted as TDoA-based relative distance estimates with respect to the first anchor.

[3] Locating a mobile node is an interesting research direction, but goes beyond the scope of this paper.

[4] In the remainder of this paper, the symbol $\hat{\zeta}$ will denote an estimate of the generic quantity ζ, e.g., calculated from experimental measurements or inferred through proper signal processing.

At each time instant, a received power measurement, e.g., the RSSI, is acquired. In order to perform target-anchor i channel status classification, N consecutive RSSI measurements are collected into the following "observation" vector:

$$\boldsymbol{z}_i^{(j)} = \left[z_i^{((j-1)N+1)}, z_i^{((j-1)N+2)}, \dots, z_i^{(jN)}\right]$$

where j is a block (of N RSSI values) time index. We assume that there are K consecutive and disjoint blocks of N RSSI values each, for a total of $K \cdot N$ overall collected RSSI samples over each link.

The target-anchor i communication channel is assumed to have the same binary status over the RSSI observation block j, and we refer to this status as

$$\ell_i^{(j)} = \begin{cases} 1 & \text{if the link is LOS} \\ 0 & \text{if the link is NLOS.} \end{cases} \tag{7}$$

We denote the collection of K consecutive observation vectors and corresponding true channel statuses as the dataset relative to the ith anchor, i.e.:

$$\mathcal{D}_i = \left\{\boldsymbol{z}_i^{(j)}, \ell_i^{(j)}\right\}_{j=1}^K \qquad i = 1, \dots, M. \tag{8}$$

In other words, $\boldsymbol{z}_i^{(1)}$ contains the first N acquired RSSI measurements associated with the true channel status $\ell_i^{(1)}$ over the link i, $\boldsymbol{z}_i^{(2)}$ contains the next N acquired RSSI measurements associated with the true channel status $\ell_i^{(2)}$ over link i, and so on for $j \in \{3, \dots, K\}$. Note that no *a-priori* information about the target-anchor i distance is contained in the dataset $\mathcal{D}_i$, $i = 1, \dots, M$. We assume that each RSSI entry in the N-sample observation vector $\boldsymbol{z}_i^{(j)}$ is a realization of a random variable $Z_i^{(j)}$ (the same for all entries of the jth block) whose statistical distribution depends on the LOS/NLOS condition of the target-anchor i link during the jth RSSI observation block, i.e., $\ell_i^{(j)}$. The dependence of $Z_i^{(j)}$ on $\ell_i^{(j)}$ would depend on the very specific propagation conditions of the associated ith link in the jth block: we give up finding an accurate statistical characterization of $Z_i^{(j)}$ but, rather, extract simple statistical features. More precisely, the dataset $\mathcal{D}_i$ will be at the basis of the extraction of relevant statistical features of the received signal to be used to classify the status of the communication channel between the target and the ith anchor.

3. Localization approach

The block diagram associated with the proposed localization approach is shown in Fig. 1. The localization method has two steps. *First*, for each anchor we process the received signal (in terms of RSSI) to classify the LOS/NLOS status of the channel (Section 3.1) and to estimate the distance from the anchor (Section 3.2 for LOS and Section 3.3 for NLOS). *Then*, "agnostic" localization algorithms are used, taking as input the link distance estimates (for all anchors) obtained from the previous step (Section 3.4).

3.1. LOS/NLOS classification

We now briefly recall the feature-based LOS/NLOS classification method proposed in [15]. Let us focus on a single target-anchor link over an observation window of N RSSI samples.[5] Given the observation vector $\boldsymbol{z} = [z^{(1)}, z^{(2)}, \dots, z^{(N)}]$ and the corresponding random variable Z (as described at the end of Section 2), let us define the kth order moment of the distribution of the random variable Z as

$$m_k = \frac{1}{N} \sum_{i=1}^{N} \left(z^{(i)} - \mu\right)^k \tag{9}$$

[5] The anchor subscript i and the observation window superscript j used in Section 2 are eliminated for notational simplicity. Therefore, the derivation refers to a generic N-sample block of consecutive RSSI values over a generic target-anchor link.

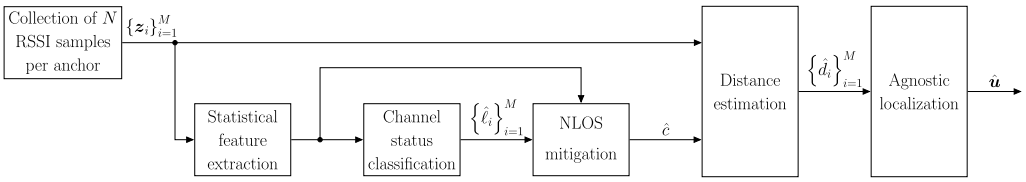

Fig. 1. Block diagram of the proposed localization approach for a generic observation window.

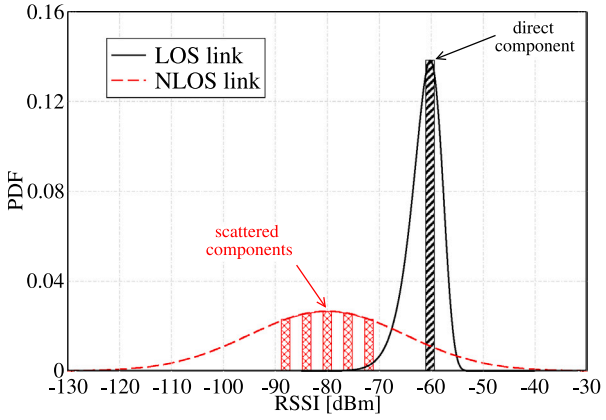

Fig. 2. Illustrative qualitative examples of RSSI distributions, for a given target location, in both LOS and NLOS link conditions.

where

$$\mu = \frac{1}{N}\sum_{i=1}^{N} z^{(i)} \tag{10}$$

is the sample mean for the observation vector. The five considered statistical features are the following:

- standard deviation σ, defined as $\sqrt{m_2}$;
- skewness S, defined as m_3/σ^3;
- kurtosis K, defined as m_4/σ^4;
- hyper-skewness $\mathscr{S}$, defined as m_5/σ^5;
- Peak Probability (PP), defined as

$$\mathscr{P} \triangleq \Pr\left\{ z^{(i)} \in \left[\max_i f\left(z^{(i)}\right) - \varepsilon, \max_i f\left(z^{(i)}\right) + \varepsilon \right] \right\}$$

where ε is a "sufficiently" small non-negative value ($\varepsilon \to 0^+$). In particular, if $\varepsilon = 0$, $\mathscr{P}$ reduces to the relative frequency of the mode value within the observation vector $\boldsymbol{z}$. Moreover, skewness, kurtosis, and hyper-skewness can be referred to as third, fourth, and fifth order standardized moments, respectively—in fact, the kth order standardized moment is defined as m_k/σ^k ($k \geq 1$).

In correspondence to the observation vector $\boldsymbol{z}$, we define the feature dataset $\tilde{D}$ as the set of statistical features extracted from $\boldsymbol{z}$ together with the true channel status ℓ, i.e.,

$$\tilde{D} = \{\sigma, S, K, \mathscr{S}, \mathscr{P}, \ell\}. \tag{11}$$

Obviously, $\tilde{D}$ depends on the (extended) dataset, defined in (8), associated with the link status and the RSSI observation block.

As outlined in [15], in LOS scenarios the direct path is characterized by a much higher received power than the reflected ones. Therefore, the RSSI distribution is expected to be peaky and *left-skewed*, and can then be well approximated by a Weibull distribution. On the other hand, in NLOS scenarios there may be several scattered and reflected paths with smaller received power. Consequently, the RSSI distribution is expected to be *symmetric* and less peaky, and can then be well approximated by a Gaussian distribution. A qualitative illustrative example of RSSI distributions, for a given target location, in both LOS and NLOS link conditions are shown in Fig. 2. Note that our work aims at determining fixed NLOS identification and mitigation parameters, representative of average NLOS conditions of the environment where the target is. This approach significantly limits the computational complexity of the localization algorithm. In other words, one has to evaluate an "average" Probability Density Function (PDF) of the RSSI in representative (in the environment where the target is placed) LOS conditions and an "average" PDF of the RSSI in representative NLOS conditions. This "training phase" allows to derive a set of features' values applicable to any LOS link and another set of features' values applicable to any NLOS link. Radically different environments are (obviously) expected to lead to different values of the features.

In [15], various classification algorithms are proposed for the identification of the link status: a Probability Mass Function (PMF)-based one; a Neural Network (NN)-based one; and a weighed threshold classifier. The first is shown to have very poor performance; on the other hand, the second is one of the possible Artificial Intelligence (AI)-based schemes suitable for such an application. In particular, a three-layer NN is considered with the following characteristics: (i) the input layer extracts the five statistical features; (ii) the hidden layer is a 8-neuron fully connected layer; and (iii) the output layer generates the estimated channel status. The activation functions for the hidden and output layers are *sigmoid* and *softmax* functions, respectively. Even if other AI algorithms can be applied (this goes beyond the scope of this paper), the NN can be considered as a reasonable state-of-the-art benchmark. In the following, we focus on the weighed threshold classifier, whose architecture is shown in Fig. 3.

The key idea is to compare each statistical feature with properly chosen threshold values $\{\sigma^*, S^*, K^*, \mathscr{S}^*, \mathscr{P}^*\}$, in order to derive the following single feature channel estimates:

$$\begin{aligned}
\hat{\ell}_\sigma &= U(\sigma^* - \sigma) \\
\hat{\ell}_S &= U(S^* - S) \\
\hat{\ell}_K &= U(K - K^*) \\
\hat{\ell}_{\mathscr{S}} &= U(\mathscr{S}^* - \mathscr{S}) \\
\hat{\ell}_{\mathscr{P}} &= U(\mathscr{P} - \mathscr{P}^*)
\end{aligned} \tag{12}$$

where $U(\cdot)$ is the unit-step function, i.e., it equals 1 for positive argument and 0 otherwise. The rationale behind (12) is that for LOS links, one expects smaller values of σ, S, and $\mathscr{S}$, and larger values of K and $\mathscr{P}$ for NLOS links. This is due to the fact that the direct component is dominant in LOS conditions, whereas the reflected paths provide a minor contribution. In particular, in LOS links, the odd-order statistical features S and $\mathscr{S}$ are expected to be negative (due to the left-skewed distribution). The chosen values of the feature thresholds depend on the considered wireless technology (namely, IEEE 802.11 and LTE) and corresponding network parameters (transmit power, RSSI resolution, etc.). However, such thresholds can be set offline to achieve the desired classification accuracy, provided that the relevant parameters are known and/or fixed in advance. As will be shown in Section 4, in our numerical results we rely on measurements taken under different conditions and we identify a unique threshold that can achieve, on average, good performance.[6]

[6] We remark that we do not aim at identifying a universal classifier for *any* scenario. Our goal is to find a "locally universal" classifier for a given scenario.

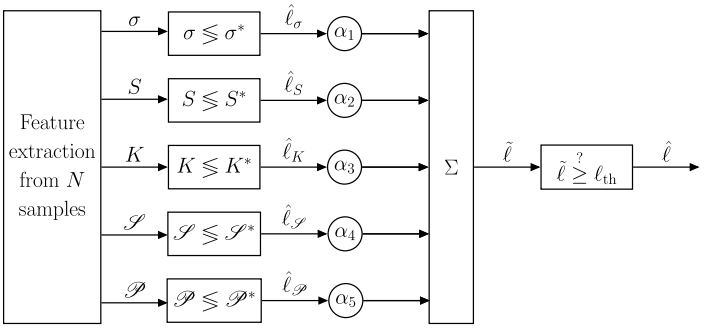

Fig. 3. Block diagram of the majority logic threshold detector for NLOS classification.

The single-feature decisions can be collected into the vector $\hat{\boldsymbol{\ell}} = [\hat{\ell}_\sigma, \hat{\ell}_S, \hat{\ell}_K, \hat{\ell}_\mathscr{S}, \hat{\ell}_\mathscr{P}]^T$. At this point, each single decision is weighed by a proper coefficient $\alpha_i \in [0,1]$, $i = 1,2,\dots,5$, to take into account possibly different reliabilities of the single decisions. Let us denote as $\boldsymbol{\alpha} = [\alpha_1, \alpha_2, \dots, \alpha_5]^T$ the vector of weighing coefficients, with $\|\boldsymbol{\alpha}\|_1 = 1$. The final decision variable $\tilde{\ell} \in [0,1]$ is

$$\tilde{\ell} = \boldsymbol{\alpha}^T \hat{\boldsymbol{\ell}} \tag{13}$$

and the channel status is finally estimated as

$$\hat{\ell} = U(\tilde{\ell} - \ell_{\text{th}}) \tag{14}$$

where $\ell_{\text{th}} \in [0,1]$ is a proper threshold. Note that if $\boldsymbol{\alpha} = 0.2 \cdot \mathbf{1}_5$, being $\mathbf{1}_n$ the all-one $n \times 1$ vector, this approach is equivalent to an unweighed majority logic threshold detector, i.e., all features have the same relevance. On the other hand, if one of the weights is equal to 1 (and, consequently, the others are 0), this rule is equivalent to a single-feature threshold detector for the feature corresponding to the unitary weight.

3.2. LOS distance estimation

Assuming the applicability of Friis formula, the estimated distance on a generic link, on the basis of the received power P_{R} (dimension: [dBm]), can be expressed as [28]

$$\hat{d} = d_0 \, 10^{\frac{P_0 - P_{\text{R}}}{10\beta}} \tag{15}$$

where P_0 is the received power (dimension: [dBm]) at the reference distance d_0 (dimension: [m]) and β is the path loss exponent (adimensional). The estimate in (15) can be applied to transmissions over channels with LOS conditions, considering $\beta = 2$. Assume that the receiver can collect RSSI samples, where RSSI is the actual power level (dimension: [dBm]) measured by the receiver.[7] Considering the average RSSI (denoted as $\overline{\text{RSSI}}$) over the observation window of N samples, the estimated distance can be approximated as follows:

$$\hat{d} \simeq d_0 \, 10^{\frac{P_0 - \overline{\text{RSSI}}}{20}}. \tag{16}$$

Note that the use of the average RSSI is expedient to eliminate statistical fluctuations (especially in experimental scenarios).

3.3. NLOS mitigation and distance estimation

As shown in Fig. 2, for a NLOS link a direct path (with dominant received power) between the transmitter and the receiver does not exist. Therefore, the electromagnetic signal travels along a longer path through reflections and/or refractions, thus reducing (with respect to the direct path) the received power. The application of (15) is critical, as the value of β would depend on the specific path. Therefore, the use of (15) with a fixed value of β (for instance, the use of (16)) may likely lead to a wrong distance estimate in NLOS conditions. To this end, we propose to mitigate the NLOS effect by deriving a more reliable link distance estimation strategy starting from (16), rather than adapting β in (15) link by link. In particular, we propose to transform a NLOS link into an "equivalent" LOS one, using a heuristic "universal" correction (independent of the specific NLOS link), as will be described in the following.

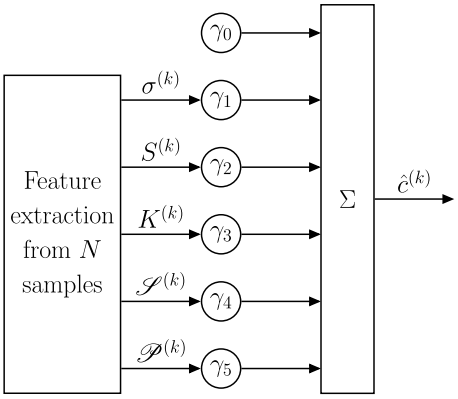

Fig. 4. Block diagram of the proposed NLOS mitigation scheme.

Let us focus on the kth observation window ($k = 1, \dots, K$) of a generic target-anchor link. When the link is classified as NLOS (according to the strategy outlined in Section 3.1), the corresponding estimated distance $\hat{d}_{\text{nlos}}$ obtained with (16) may be heuristically corrected by means of a scalar coefficient as

$$\hat{d}^{(k)}_{\text{nlos-c}} = \frac{\hat{d}^{(k)}_{\text{nlos}}}{\hat{c}^{(k)}} \tag{17}$$

where $\hat{d}^{(k)}_{\text{nlos-c}}$ is the estimated distance after the correction and $\hat{c}^{(k)} > 1$ is a proper correction parameter, which quantifies the NLOS effect. In particular, the correction coefficient at the kth time epoch can be empirically computed as a linear regression, with proper coefficients, of the statistical features extracted online from the current block of N RSSI samples. In other words,

$$\hat{c}^{(k)} = \boldsymbol{\gamma}^T \boldsymbol{f}^{(k)} \tag{18}$$

A pictorial description of the NLOS mitigation scheme is provided in Fig. 4.

The regression weight vector $\boldsymbol{\gamma}$ can be computed offline during a system calibration phase as follows. Assume that the target is placed at known pre-defined positions, so that L estimated distances associated

Different scenarios would require to identify a proper threshold by averaging over various conditions.

[7] This assumption is typical for IoT devices. Moreover, in most cases the available RSSI values are quantized.

with NLOS links are available[8] and collected in the vector $\hat{\boldsymbol{d}}_{\text{nlos}} = [\hat{d}^{(1)}_{\text{nlos}}, \ldots, \hat{d}^{(L)}_{\text{nlos}}]^T$. Assume also that the corresponding true distances are known and collected in the vector $\boldsymbol{d}_{\text{true}} = [d^{(1)}, \ldots, d^{(L)}]^T$. The statistical features over the entire observation window can be collected in the following $L \times 6$ matrix:

$$\boldsymbol{F} = \left[\boldsymbol{f}^{(1)^T}, \boldsymbol{f}^{(2)^T}, \ldots, \boldsymbol{f}^{(L)^T}\right]^T. \tag{19}$$

The optimal weight vector solves the following minimization problem:

$$\boldsymbol{\gamma} = \underset{\boldsymbol{a}=[a_0,\ldots,a_5]^T}{\arg\min} \left\| \boldsymbol{d}_{\text{true}} - \hat{\boldsymbol{d}}_{\text{nlos}} \odot \frac{1}{\boldsymbol{F}\,\boldsymbol{a}} \right\| \tag{20}$$

where $\odot$ denotes element-wise vector multiplication. In other words, the weight vector minimizes the error between the true distance and the corrected one. In order to make the calibration method accurate, the total number L of collected RSSI blocks must be sufficiently large. From a practical point of view, this corresponds to considering a sufficiently large number of NLOS links (sufficiently heterogeneous) with known distances and carry out data collection. The weight vector $\boldsymbol{\gamma}$ will then be used, during online operations, if a link is identified as NLOS. The identification of an efficient calibration dataset (in terms of set of L NLOS links) is an interesting research problem.

Obviously, this approach applies to a given scenario of interest. Should the scenario change (significantly), calibration should be carried out again.

3.4. "Agnostic" localization

Once the estimated distances are available from all the M anchors, an "agnostic" localization algorithm can be run to derive a final target position estimate. The algorithm is agnostic in the sense that it acts as if all links were LOS. In fact, a NLOS link is transformed into an equivalent LOS one according to the steps discussed in Sections 3.1 and 3.3.

In general, a localization algorithm solves a system of equations of the type shown in (4). As illustrative (but not exhaustive) examples of agnostic localization algorithms, we now briefly recall two geometric algorithms, namely Two-Stage Maximum-Likelihood (TSML) [29] and Plane Intersection (PI) [30], which will be used for localization purposes. In particular, TDoA-based implementation of TSML and PI are considered. Besides geometric solutions, Particle Swarm Optimization (PSO)-based solutions will also be considered. An exhaustive analysis of RSSI-based least squares lateration algorithms is presented in [31].

We remark that the localization accuracy of ToA-based algorithms, not shown here for lack of space, is lower than that of TDoA-based ones. Even if ToA-based processing may be more attractive from an implementation point of view, we focus on TDoA-based processing, which guarantees the best performance. In this case, inter-anchor synchronization is crucial: in IoT scenarios, this can be delegated to the infrastructure, i.e., to the cooperating anchors. The investigation of this aspect goes beyond the scope of this paper, see, e.g., [32] and references therein.

3.4.1. Two-stage maximum-likelihood (TSML)

The TSML algorithm resorts to a two-step approach and solves, in each step, a smaller system of equations (with respect to the starting one) [29]. Defining the unknown vector as $\boldsymbol{\phi}_1 = \left[\boldsymbol{u}^T, d_1\right]^T$, one obtains the following system of equations for the first step:

$$\boldsymbol{G}_1\boldsymbol{\phi}_1 = \boldsymbol{h}_1 \tag{21}$$

where $\boldsymbol{G}_1$ is a $(M-1)\times 3$ matrix and $\boldsymbol{h}_1$ is a length-$(M-1)$ vector defined as follows:

$$\boldsymbol{G}_1 = -2\begin{bmatrix} x_2 - x_1 & y_2 - y_1 & \hat{\Delta}_2 \\ \vdots & \vdots & \vdots \\ x_M - x_1 & y_M - y_1 & \hat{\Delta}_M \end{bmatrix} \tag{22}$$

$$\boldsymbol{h}_1 = \begin{bmatrix} k_1^2 - k_2^2 + \hat{\Delta}_2^2 \\ \vdots \\ k_1^2 - k_M^2 + \hat{\Delta}_M^2 \end{bmatrix}. \tag{23}$$

As $\boldsymbol{G}_1$ is not a square matrix, the solution $\hat{\boldsymbol{\phi}}_1$ can be obtained, by resorting to a Least Squares (LS) method [33], as follows:

$$\hat{\boldsymbol{\phi}}_1 = \left(\boldsymbol{G}_1^T\boldsymbol{G}_1\right)^{-1}\boldsymbol{G}_1^T\boldsymbol{h}_1. \tag{24}$$

At this point, since the third unknown in $\boldsymbol{\phi}_1$ (namely, d_1) depends on the other two (namely, $\boldsymbol{u}$), one has to solve a system of equations to eliminate this dependence. Denoting $\boldsymbol{\phi}_2 = (\boldsymbol{u} - \boldsymbol{s}_1)^2$, the following final system of equations has to be solved:

$$\boldsymbol{G}_2\boldsymbol{\phi}_2 = \boldsymbol{h}_2 \tag{25}$$

where $\boldsymbol{G}_2$ is a 3×2 matrix, whereas $\boldsymbol{h}_2$ is a length-3 vector defined, respectively, as follows:

$$\boldsymbol{G}_2 = \begin{bmatrix} 1 & 0 \\ 0 & 1 \\ 1 & 1 \end{bmatrix} \tag{26}$$

$$\boldsymbol{h}_2 = \left(\hat{\boldsymbol{\phi}}_1 - \left[\boldsymbol{s}_1^T, 0\right]^T\right)^2. \tag{27}$$

The LS solution is then

$$\hat{\boldsymbol{\phi}}_2 = \left(\boldsymbol{G}_2^T\boldsymbol{G}_2\right)^{-1}\boldsymbol{G}_2^T\boldsymbol{h}_2 \tag{28}$$

and the final position estimate is obtained combining $\hat{\boldsymbol{\phi}}_1$ and $\hat{\boldsymbol{\phi}}_2$ according to

$$\hat{\boldsymbol{u}} = \text{sign}\left(\breve{\boldsymbol{\phi}}_1 - \boldsymbol{a}_1\right) \odot \hat{\boldsymbol{\phi}}_2 + \boldsymbol{a}_1 \tag{29}$$

where sign$(\cdot)$ represents the sign operator and $\breve{\boldsymbol{\phi}}_1$ is a bi-dimensional vector formed by the first two vector components of $\hat{\boldsymbol{\phi}}_1$.

Note that evaluating (24) has complexity on the order of $O(M^2)$ [34]. On the other hand, the solution of (28) leverages operations on small-size matrices and vectors, with negligible computation complexity, especially in the presence of a large number of anchors.

3.4.2. Plane intersection (PI)

The rationale behind this approach is that any pair of TDoA measurements, coming from a group of three anchors, leads to an equation which identifies the major axes of a conic, whose focus should lie in the target [30]. Therefore, having at least three of these equations allows to determine the target position by solving the corresponding system of equations.[9]

The system of equations to be solved is

$$\boldsymbol{A}\,\boldsymbol{u} = \boldsymbol{b} \tag{30}$$

where $\boldsymbol{A}$ is a $(M-2)\times 2$ matrix and $\boldsymbol{b}$ is a length-$(M-2)$ vector defined as follows:

$$\boldsymbol{A} = \begin{bmatrix} (x_1 - x_2)\hat{\Delta}_3 - (x_1 - x_3)\hat{\Delta}_2 & (y_1 - y_2)\hat{\Delta}_3 - (y_1 - y_3)\hat{\Delta}_2 \\ \vdots & \vdots \\ (x_1 - x_2)\hat{\Delta}_M - (x_1 - x_M)\hat{\Delta}_2 & (y_1 - y_2)\hat{\Delta}_M - (y_1 - y_M)\hat{\Delta}_2 \end{bmatrix} \tag{31}$$

$$\boldsymbol{b} = \begin{bmatrix} -\hat{\Delta}_2\,\hat{\Delta}_3(\hat{\Delta}_3 - \hat{\Delta}_2) + (k_1^2 - k_2^2)\hat{\Delta}_3 - (k_1^2 - k_3^2)\hat{\Delta}_2 \\ \vdots \\ -\hat{\Delta}_2\,\hat{\Delta}_M(\hat{\Delta}_M - \hat{\Delta}_2) + (k_1^2 - k_2^2)\hat{\Delta}_M - (k_1^2 - k_M^2)\hat{\Delta}_2 \end{bmatrix}. \tag{32}$$

[8] L consecutive N RSSI samples' blocks are collected sequentially.

[9] Note that, in this case, a second reference anchor is needed to determine the system of equations. To this end, for notation simplicity, we will assume that $\boldsymbol{s}_2$ is the second anchor closest to the target.

Hence, the LS solution can be computed as

$$\hat{\boldsymbol{u}} = \left(\boldsymbol{A}^T \boldsymbol{A}\right)^{-1} \left(\boldsymbol{A}^T \boldsymbol{b}\right) \tag{33}$$

with complexity on the order of $O(M^2)$ [34] (similar arguments to those for TSML can be applied).

3.4.3. Particle swarm optimization (PSO)

The previously outlined geometric-based algorithms (TSML and PI) analytically solve the systems of equations described above. However, it may happen that the matrices involved in these systems of equations become ill-conditioned, thus leading to a very inaccurate target position estimate [35,36]. The rationale behind the use of the PSO algorithm is to re-interpret the above systems of equations as minimization problems, avoiding numerical problems in finding their solutions. More precisely, the solution of the general localization problem (4) can be written as

$$\hat{\boldsymbol{u}} = \arg\min_{p} g(\boldsymbol{\rho}) \qquad \boldsymbol{\rho} \in \mathbb{R}^2 \tag{34}$$

where $g(\cdot)$ is the so-called fitness function and depends on the starting system of equations.

The fitness function should take into account the error, in the system of equations, when a wrong position is estimated: in particular, the larger the error, the higher the value of the fitness function. Starting from (21) for the TSML algorithm, the following fitness function can be considered:

$$g(\boldsymbol{\rho}) = \left\| \hat{\boldsymbol{\Delta}}^2 - (k^2 - k_1^2) + 2\,\hat{\boldsymbol{\Delta}} \left\| \boldsymbol{\rho} - \boldsymbol{s}_1 \right\| + 2\,(\boldsymbol{S} - \boldsymbol{s}_1)^T \boldsymbol{p} \right\| \tag{35}$$

where $\hat{\boldsymbol{\Delta}}^2$ stands for the element-wise square of the vector $\hat{\boldsymbol{\Delta}}$. We refer to the PSO solution of (35) as PSO-TSML. Note that (35) provides a solution which is "biased" towards the first anchor $\boldsymbol{s}_1$, especially for large values $\hat{\boldsymbol{\Delta}}$, due to the presence of the term $2\,\hat{\boldsymbol{\Delta}} \left\| \boldsymbol{\rho} - \boldsymbol{s}_1 \right\|$.

If, instead of the system given by (21), the system given by (30) is considered for the PI algorithm, the following fitness function can be used:

$$g(\boldsymbol{\rho}) = \left\| \boldsymbol{b} - \boldsymbol{A}\,\boldsymbol{\rho} \right\|. \tag{36}$$

We refer to the PSO solution of (36) as PSO-PI.

At this point, we resort to the standard implementation of the PSO (see, e.g., [37]) to solve the minimization problem (34) with fitness function equal either to (35) or (36). According to the PSO algorithm, the set of potential solutions of each optimization problem, i.e., of the system of equations associated with the chosen localization algorithm, can be modeled as a swarm of particles. We denote the set of particles as $\mathcal{P}$ and its size as $|\mathcal{P}|$. The positions of the particles are randomly initialized in the region of interest and the key idea is to iteratively "guide" them towards the optimal solution by exploring the interactions between them.

At iteration[10] n ($n = 0, 1, \ldots, n_{\text{it}}$, where n_{it} is the number of iterations), the position and velocity of the ith particle are represented by the two-dimensional vectors $\boldsymbol{\pi}_i[n]$ and $\boldsymbol{v}_i[n]$, respectively. The PSO algorithm assumes that each particle knows, at each iteration, its own best position (as will be discussed in the following) as well as the global best position among all the particles and the corresponding values of the fitness function.

The update rule for particles' velocities is given by

$$\boldsymbol{v}_i[n+1] = \omega[n]\,\boldsymbol{v}_i[n] + c_1\,\chi_1[n]\left\{\boldsymbol{p}_i[n] - \boldsymbol{\pi}_i[n]\right\} + c_2\,\chi_2[n]\left\{\boldsymbol{p}[n] - \boldsymbol{\pi}_i[n]\right\} \tag{37}$$

where: ω is the PSO inertial factor; c_1 and c_2 ($c_1, c_2 \in \mathbb{R}$, $c_1, c_2 \geq 0$) are the so-called *cognition* and *social* parameters; and $\chi_1[n]$ and $\chi_2[n]$ are independent random variables uniformly distributed in $[0, 1]$. Finally, $\boldsymbol{p}_i[n]$ and $\boldsymbol{p}[n]$ represent, respectively, the position of the ith particle with the best fitness function (over the n iterations) and the position of the particle with the best (among all particles) fitness function up to iteration n, i.e.,

$$\boldsymbol{p}_i[n] = \arg\min_{\boldsymbol{\rho} \in \{\boldsymbol{\pi}_i[j]\}_{j=0}^{n}} g(\boldsymbol{\rho})$$

$$\boldsymbol{p}[n] = \arg\min_{\boldsymbol{\rho} \in \{\boldsymbol{p}_i[n]\}_{i=1}^{|\mathcal{P}|}} g(\boldsymbol{\rho}).$$

Using (37), the update rule for the particles' positions is

$$\boldsymbol{\pi}_i[n+1] = \boldsymbol{\pi}_i[n] + \boldsymbol{v}_i[n+1].$$

In other words, the idea of the PSO algorithm is to check the system of equations in correspondence to some test positions, find the position with best fitness, and try to iteratively converge to the best position, by also exploring other positions in the surrounding space. The final solution is given by

$$\hat{\boldsymbol{u}} = \arg\min_{\boldsymbol{\rho} \in \{\boldsymbol{p}_i[n_{\text{it}}]\}_{i=1}^{|\mathcal{P}|}} g(\boldsymbol{\rho}).$$

As a final remark, one can note that the inertial factor $\omega[n]$ is representative of the ability of the particles to explore new areas in the surrounding space. However, taking into account the results in [35], in the following we will consider $\omega[n] \simeq 0\ \forall n$ in (37).

Since at each iteration the fitness function has to be evaluated for all particles, it can be shown that the complexity is $O(|\mathcal{P}| \cdot n_{\text{it}} \cdot M)$ [34]. Since $|\mathcal{P}|, n_{\text{it}} \gg M$, the complexity of this algorithm may be unfeasible in most realistic applications with computational and (possibly) latency constraints (e.g., those involved in IoT scenarios).

4. Experimental performance analysis

We now present an experimental performance analysis in IEEE 802.11 (indoor) and LTE (outdoor) wireless scenarios. The indoor scenario is shown in Fig. 5 and corresponds to the WiFi network deployed at the ground floor of the Building n. 2 of the Department of Engineering and Architecture of the University of Parma, Italy. The six anchors (denoted by blue circles) are IEEE 802.11 Cisco AIR-CAP3702I-E-K9 APs transmitting over 3 disjoint IEEE 802.11 20 MHz bandwidth channels (channels 1, 6, and 11). On the other hand, the target (denoted by a red cross/circle/diamond and placed in 3 illustrative positions) is shown in Fig. 6 and corresponds to a Raspberry Pi 3 Model B+ (RPi) Single Board Computer (SBC), equipped with (i) an external IEEE 802.11 Linksys TL-WN722N USB dongle, with a 1 dB granularity RSSI measurement capability, and (ii) an *on-board*-plugged Waveshare SIM7600E-H 4G HAT expansion board, with a 1 dB granularity RSSI measurement capability. In the RPi, Wireshark is running to extract RSSI measurements from the beacon packets received by the APs. For each target position, the corresponding LOS/NLOS links are listed in Table 1. LOS is associated with direct visibility, whereas NLOS is associated with the presence of at least one large obstructive object between target and anchor (e.g., wall, thick door, cabinet). Then, measurements are taken under different conditions (e.g., at various hours with different WiFi traffic loads, people passing by, etc.). Note that all the positions have the same number (namely, 2) of links in NLOS conditions.

In the LTE outdoor scenario, the anchors are evolved Node Bs (eNBs) transmitting with an uplink frequency equal to 847 MHz and a downlink frequency equal to 806 MHz, over a bandwidth of 10 MHz. The target corresponds to the aforementioned IoT node in Fig. 6 running a proper script which collects RSSI data through the LTE hat's internal

[10] The use of an inherently iterative algorithm leads to a delay in the estimation procedure, which may be critical (depending on the available computation hardware) for real-time applications or dynamic scenarios with mobile targets. The investigation of refined techniques to reduce the number of iterations in conjunction with target tracking will be subject of future investigation.

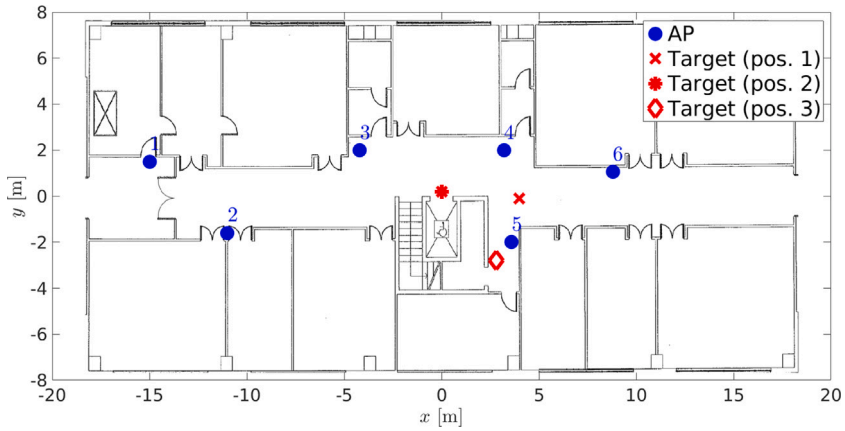

Fig. 5. Indoor WiFi-based localization scenario, with three possible target positions.

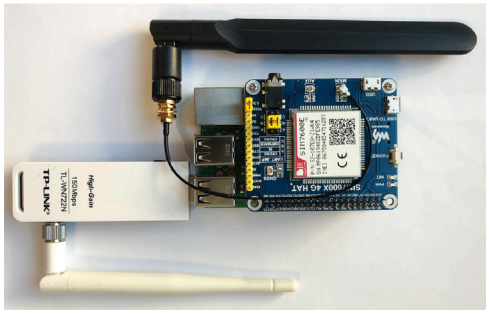

Fig. 6. IoT target node used for the experimental performance analysis in indoor and outdoor localization scenarios.

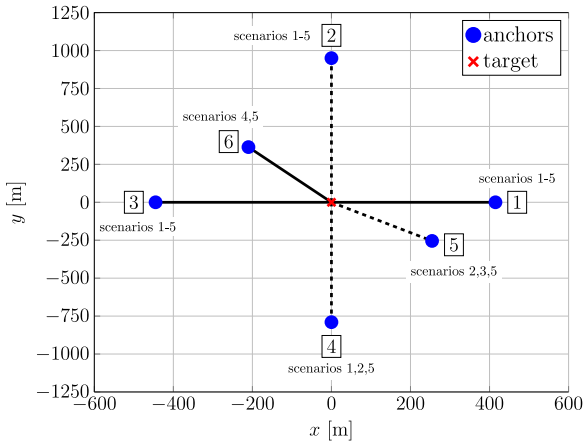

Fig. 7. Outdoor LTE-based "virtual" localization scenarios: LOS links are indicated with solid lines and NLOS links are indicated with dashed lines. The target position is fixed and, next to each anchor, the scenarios where the anchor is involved are indicated.

Application Programming Interfaces (APIs). Since the available APIs do not allow for simultaneous data collection from several eNBs, we collect single link measurements from a single eNB under different LOS/NLOS channel conditions and then build a "virtual" scenario, as shown in Fig. 7, where solid and dashed lines correspond to LOS and NLOS links, respectively. The virtual scenario is obtained by placing "virtual" eNBs at distances, from the target, equal to the distances from the real eNB at which real experimental data were collected. Moreover, for each virtual eNB, LOS or NLOS channel status is selected on the basis of the corresponding experimental data: LOS is associated with direct visibility of anchors and target, whereas a NLOS status is

Table 1
Configurations of LOS and NLOS links for the considered three experimental WiFi-based indoor scenarios. The target-anchor (AP) links are LOS/NLOS depending on the position of the target.

Scenario (target position)	LOS links	NLOS links	Not considered anchors
1	3,4,5,6	1,2	–
2	3,4	2,5	1,6
3	4,5	3,7	1,2,6

Table 2
Configurations of LOS and NLOS links for the considered "virtual" LTE-based outdoor scenarios. The target is fixed and the status (LOS/NLOS) of each link depends on the anchor (eNB). Each scenario involves a different configuration of anchors.

Scenario	LOS links	NLOS links	Not considered anchors
1	1,2	3,4	5,6
2	1,2	3,4,5	6
3	1,2	3,5	4
4	1,2,6	3	5
5	1,2,6	3,4,5	–

associated with the presence of either the target inside a building or with the presence of at least one building between target and anchor. In particular, the data associated with link between the ith virtual anchor ($i = 1, 2, \ldots, 6$) and the target corresponds to the measured RSSI values at the ith eNB-target distance under different LOS/NLOS conditions. As for the indoor scenario, in this case as well measurements are taken under different environmental conditions for fixed target-eNBs' distances and LOS/NLOS conditions (e.g., node inside a building, presence of thick walls, etc.). The considered scenarios (with different LOS/NLOS conditions) are described in Table 2. Unlike the indoor case, in the outdoor case the target is fixed and the links statuses depend on the "virtual" anchor. Different scenarios involve different configurations of anchors.

In both cases, data are collected at the target with a RSSI sampling interval of 100 ms. The number T of collected RSSI blocks from all the anchors is 842 for WiFi and 757 for LTE, each block containing $N = 30$ consecutive RSSI samples, corresponding to an observation time of 3 seconds. Note that this interval may be too large for scenarios where the target is a moving person. However, the focus of the proposed approach is on IoT applications in which the nodes are *quasi*-static and, therefore, the communication channel experiences limited variations. Note also that the overall acquisition time can be farther reduced, for a fixed value of N, with a shorter sampling interval, i.e., higher sampling rate. As preliminarily shown in [15], the accuracy of NLOS identification improves if N increases. Consequently, the performance of the mitigation can improve as well, since the NLOS links can be identified more accurately. However, increasing N leads to a longer delay in the acquisition process: this can be critical in dynamic scenarios with a

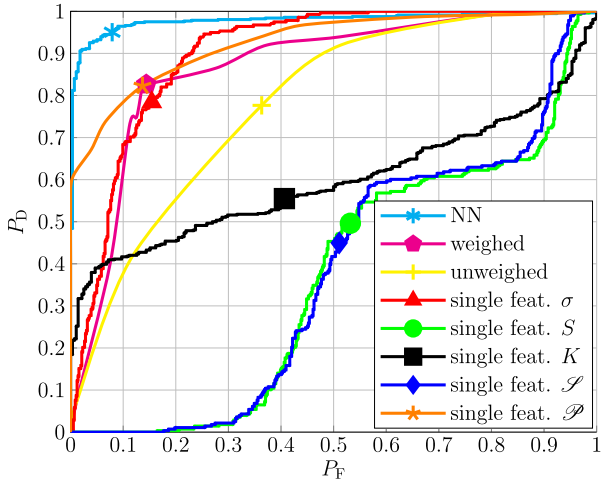

Fig. 8. ROC curves of the considered classifiers in the indoor WiFi scenario with the target in position 1 (see Fig. 5 and Table 1). For each curve, the marker shows the working point for final classification accuracy of approximately 84%.

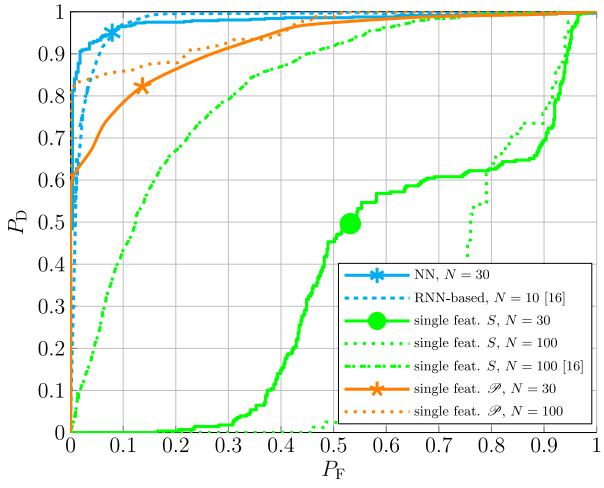

Fig. 9. ROC curves of some of the proposed classifiers in the indoor WiFi scenario (position 1, see Fig. 5 and Table 1) and various values of N. A comparison with the classifiers in [16] is provided.

mobile target. In this case, in fact, if the acquisition delay is too long, the LOS/NLOS classification may refer to an outdated target position and may make the entire localization process inaccurate. Our results (with various values of N), not presented here for lack of space, show that $N = 30$ is a good trade-off between position estimation accuracy and delay. The number L of blocks of RSSI measurements associated with NLOS links is 278 for the WiFi scenario and 405 for the LTE scenario. Therefore, the number $T - L$ of blocks associated with LOS links is 564 for the WiFi case and 352 with LTE.

Channel classification is performed for each of the T blocks of RSSI measurements—channel status is considered constant over a block. When the reference NN classifier is considered, the input layer extracts the set of features $\tilde{D}$, while the output generates the estimated channel status $\hat{\ell}$. Internally, the hidden layer is a 5-neuron fully connected layer using the scaled conjugate gradient training function. The size of the training, validation, and testing dataset are 80%, 10%, and 10% of T, respectively [15]. These values are chosen as a reasonable trade-off between training duration and NN performance. Moreover, cross-validation has been performed by considering different subsets' training, validation, and testing and, then, computing the average performance.

Table 3
Parameters for NLOS classification and mitigation in the indoor WiFi scenario with the target in position 1 (see Fig. 5 and Table 1).

Feature	Threshold	Classification weights	Mitigation weights ($\gamma_0 = -1.39$)
σ	$\sigma^* = 2$	$\alpha_1 = 0.2$	$\gamma_1 = 0.56$
S	$S^* = 0.6$	$\alpha_2 = 0.1$	$\gamma_2 = -1.59$
K	$\mathscr{K}^* = 5$	$\alpha_3 = 0.1$	$\gamma_3 = 0.31$
$\mathscr{S}$	$\mathscr{S}^* = 5$	$\alpha_4 = 0.1$	$\gamma_4 = 0.04$
$\mathscr{P}$	$\mathscr{P}^* = 0.7$	$\alpha_5 = 0.5$	$\gamma_5 = 3.40$

Regarding channel mitigation, the regression weight vector $\boldsymbol{\gamma}$ in (20) is computed using all the L blocks of the NLOS measurements to generate the matrix $\boldsymbol{F}$ in (19). Then, this vector is used to compute the distance correction coefficient for the specific link and block according to (18). Note that this training operation, including the computation of the thresholds for NLOS classification, occurs only once at the deployment of the localization system.

Finally, a localization act is performed every time the target acquires a block of $N = 30$ RSSI measurements from each of the M anchors (i.e., after $N \cdot M$ RSSI values are acquired)—the values of M depend on the specific scenario (see Tables 1 and 2). The total number of performed localization acts, denoted as K', is between 100 and 150 and depends on two aspects: (i) the number of times that the target is able to collect data from the all the anchors; and (ii) the application (or not) of an outlier removal strategy. In particular, the acquisition of the set of $N \cdot M$ RSSI values is stopped when a sufficient number of localization acts can be performed also in the presence of outlier removal. Regarding the outlier removal strategy, in this work we *a-priori* assume that the position estimate should lie inside the polytope identified by the anchors, i.e., the anchors should be at the boundary of the monitored area. Therefore, the considered outlier removal strategy eliminates position estimates that are significantly outside such a polytope.[11] In particular, we discard decisions for which $|\hat{x}_j| > 2\max_i |\boldsymbol{s}_i|$ or $|\hat{y}_j| > 2\max_i |\boldsymbol{s}_i|$, where $\hat{x}_j$ and $\hat{y}_j$ are the coordinates of the position estimate $\hat{\boldsymbol{u}}_j$ at the jth localization act. For example, this could be appropriate for in-region user presence verification. Note that the outlier removal strategy only affects the localization algorithm and not the NLOS identification stage. In the indoor WiFi scenarios, the percentage of outliers is between 0% (for PSO-TSML) and 27% (for TSML), whereas it ranges between 0% (for PSO-TSML) and 50% (for TSML) in the outdoor LTE scenarios.

4.1. Indoor WiFi scenarios

We first analyze the performance of the NLOS classifier in terms of its Receiver Operating Characteristic (ROC) curve, defined as the probability of correct LOS classification, i.e., $P_D = P(\hat{\ell} = 1|\ell = 1)$, as a function of the probability of incorrect NLOS classification, i.e., $P_F = P(\hat{\ell} = 1|\ell = 0)$. The ROC curve for the indoor WiFi scenario is shown in Fig. 8, considering various classifiers and the target in position 1 (see Fig. 5). For each considered classifier, the ROC curve is composed of points associated with different decision strategies, namely the values of single thresholds for the single-feature classifiers and $\tilde{\ell}_{\text{th}}$ for the weighed classifier. The markers on the curves (one per curve) show the operational points in correspondence to which the final classification accuracy is approximately 84%.[12] The values of the thresholds and weights of the various classifiers needed to achieve a final classification accuracy of approximately 84% are shown in Table 3. In this case, $\ell_{\text{th}} = 0.5$.

[11] Improved outlier removal strategies can be considered, but this goes beyond the scope of this paper.

[12] This value is chosen as a reasonable performance trade-off.

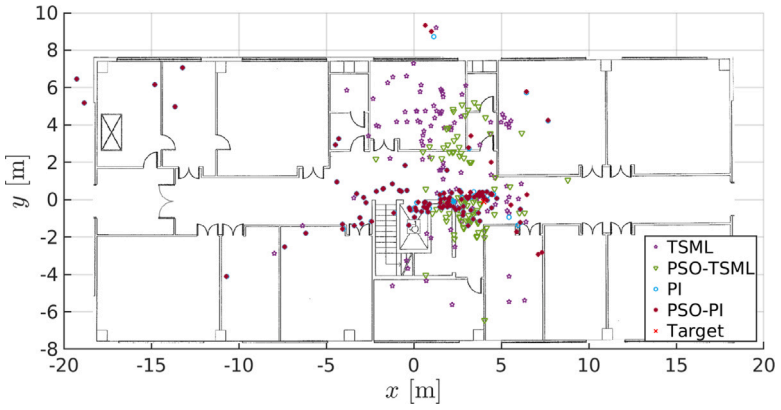

Fig. 10. Estimated positions in indoor WiFi scenario (position 1, see Fig. 5 and Table 1) with outlier removal.

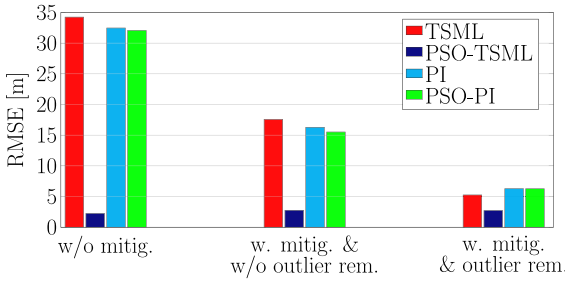

Fig. 11. RMSE for the indoor WiFi scenario and position 1 (see Fig. 5 and Table 1).

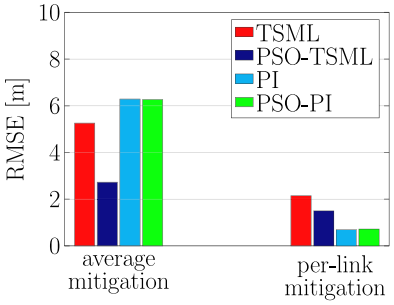

Fig. 12. RMSE for the considered indoor WiFi-based scenario (position 1, see Fig. 5 and Table 1), comparing the average mitigation with per-link optimized mitigation.

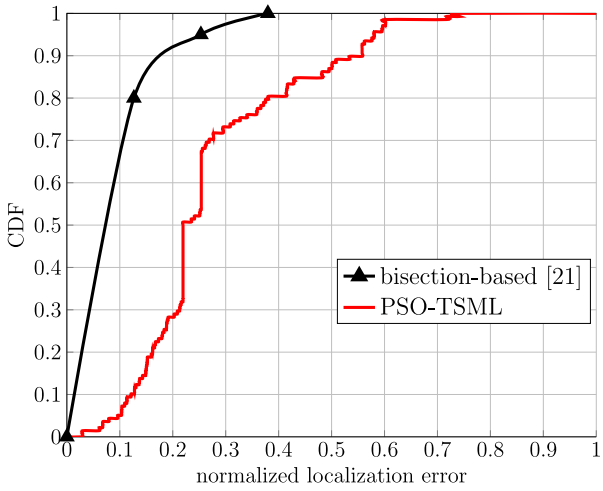

Fig. 13. CDF of the localization error normalized to the average anchor-target distance, comparing the PSO-TSML (our best performing algorithm with WiFi communications) with the experimental performance of the bisection-based algorithm detailed in [21] using 6 anchors and UWB communications.

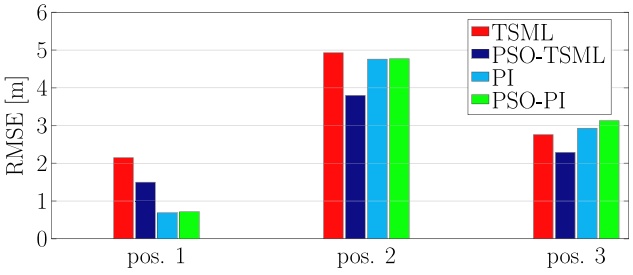

Fig. 14. RMSE results for indoor WiFi scenario and different positions of the target (see Fig. 5 and Table 1).

As can be seen from the results in Fig. 8, the NN-based classifier provides the best solution, yet paying a higher price in terms of computational complexity and training needs. Moreover, for a final classification accuracy of 84%, properly weighing all the five considered features allows to achieve the best performance among the considered classifiers. However, the single-feature classifiers based on PP or σ achieve very good results (for instance, the performance with PP at 84% accuracy overlaps with the performance with weighing) with a very simple implementation. This behavior makes single-feature classifiers attractive for energy conservation purposes (especially for mobile and constrained devices, such as in IoT-oriented scenarios). On the other hand, other single-feature classifiers (based on S, K and $\mathscr{S}$) do not provide acceptable performance.

In Fig. 9, we compare our classification results in the indoor WiFi scenario (considering two values of N, namely 30 and 100) with those in [16], where the following approaches have been considered: (i) a reference case with Recurrent Neural Network (RNN) and $N = 10$ and (ii) a single statistical feature (namely the skewness) classifier with $N = 100$. One can observe that the NN (ours) and RNN [16] benchmarks have similar performance. Moreover, our single-feature classifier (based on the PP) with $N = 30$ outperforms single-feature classifier (based on skewness) of [16] with $N = 10$. Note that our accuracy, precision, and sensitivity results are in agreement with those in [25, Table 1].

After classification, NLOS mitigation is carried out. In Table 3, the weights for the mitigation procedure, corresponding to each feature, are shown.

After mitigation of the 2 NLOS links associated to anchors 1 and 2 (see Fig. 5), localization is carried out. The estimated positions are shown in Fig. 10. As a concise performance indicator of the localization accuracy, we evaluate the Root Mean Square Error (RMSE, dimension:

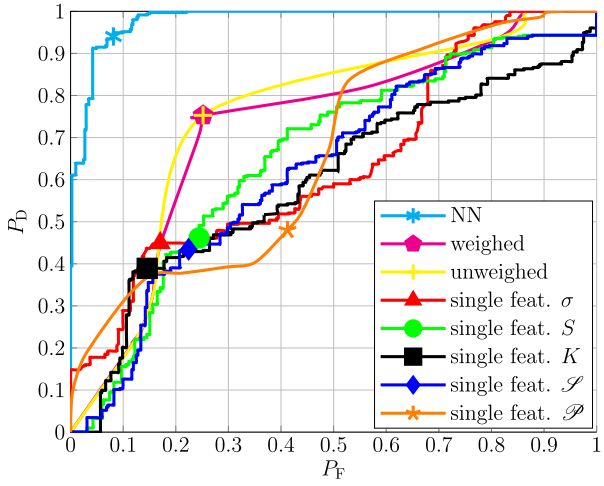

Fig. 15. ROC curves of the considered classifiers in the outdoor LTE scenario 1 (see Fig. 7 and Table 2). For each curve, the marker shows the working point for final classification accuracy of approximately 75%.

[m]), defined as

$$\text{RMSE} = \sqrt{\frac{1}{K'}\sum_{j=1}^{N}\left|\boldsymbol{u}-\hat{\boldsymbol{u}}_j\right|^2}.$$

The RMSE results are shown in Fig. 11 for the indoor WiFi scenario. The case without and with NLOS mitigation are compared. In the latter case, we show the results for both the cases without and with outlier removal. One can observe that our (pre-localization) NLOS mitigation strategy significantly reduces the RMSE, especially if carried out with outlier removal. The only exception is the PSO-TSML algorithm, which performs well also in the absence of correction, provided that a sufficient number of particles and iterations are performed. However, as previously observed, the complexity of a PSO-based solution is typically high and, therefore, the adoption of such a solution is unfeasible in IoT scenarios. Moreover, PSO requires an iterative process, which may also hinder its applicability from a latency point of view. However, PSO-TSML represents a relevant performance benchmark. In fact, the latency is caused by the localization algorithm, but the initial training phase to determine the parameters for NLOS identification and mitigation is the same as for the other algorithms.

While our approach entails a fixed mitigation parameter $\boldsymbol{\gamma}$ in (20), valid for all links, it is of interest to compare its performance with that obtained in the case in which NLOS identification and mitigation parameters are optimized for each target-anchor communication link. In Fig. 12, the RMSE is shown for the considered indoor WiFi scenario, comparing our "average mitigation" with per-link optimized mitigation. In all the cases, NLOS correction and outlier removal is considered. As expected, the localization accuracy improves when the mitigation coefficient is optimized for each NLOS link. In particular, the PI is the algorithm which mostly benefits from NLOS mitigation. However, this comes at the price of an increased complexity and no scalability, since one has to train the system for each specific link.

We now compare our performance with that of [21], considered as a literature benchmark. In Fig. 13, the Cumulative Distribution Function (CDF) of the localization error, normalized to the average anchor-target distance, is shown, comparing the PSO-TSML (namely, the algorithm with the best performance with our approach) with the experimental results of [21] using 6 anchors. One can observe that the performance of our scheme is aligned with that of [21], even if the latter uses a different NLOS model (with constant bias) and UWB signaling (which achieves a significantly higher ranging accuracy). In particular, with probability equal to 80%, the error with UWB is around

Table 4
Parameters for NLOS classification and mitigation in the outdoor LTE scenario 1 (see Fig. 7 and Table 2).

Feature	Threshold	Classification weights	Mitigation weights ($\gamma_0 = -0.62$)
σ	$\sigma^* = 1.7$	$\alpha_1 = 0.2$	$\gamma_1 = 5.58$
S	$S^* = 0$	$\alpha_2 = 0.2$	$\gamma_2 = -1.83$
K	$\mathscr{K}^* = 3$	$\alpha_3 = 0.3$	$\gamma_3 = 6.51$
$\mathscr{S}$	$\mathscr{S}^* = -0.1$	$\alpha_4 = 0.2$	$\gamma_4 = -7.88$
$\mathscr{P}$	$\mathscr{P}^* = 0.7$	$\alpha_5 = 0.1$	$\gamma_5 = 0.71$

12% of the average target-anchor distance, whereas with WiFi is around 37%. Moreover, our strategy has the advantage of being agnostic to the considered localization algorithm, whereas the approach in [21] requires to change the entire localization procedure.

We finally show in Fig. 14 the performance, in terms of RMSE, for different target positions (see Fig. 5). Note that positions 2 and 3 show a higher localization error, due to the smaller number of employed anchors in the localization process (i.e., 4 anchors instead of 7). Moreover, NLOS classification accuracy worsens, especially with the target in position 2 .

4.2. Outdoor LTE scenarios

We now analyze the performance in the outdoor LTE scenario. We first consider scenario 1 (see Fig. 7 and Table 2). The ROC curves for the considered classifiers are shown in Fig. 15. Considerations similar to those carried out for Fig. 8 are still valid, except for the fact that, in general, link classification and, therefore, NLOS mitigation is less accurate. In Fig. 15, the operational points indicated with a symbol over the ROC curves correspond to a final localization accuracy of 75% (the highest with LTE). As can be seen, the weighed classifiers (both using all features) allow to achieve the best performance (for a final accuracy of 75%), whereas the performance with the single-feature classifiers degrades. Therefore, the weighed classifier can be considered as "universal", in the sense that it allows to achieve almost the best performance in both (indoor and outdoor) considered scenarios—obviously, by properly setting the algorithms' parameters according to the scenario. The thresholds and weights of the NLOS classifier, to achieve a final classification accuracy of approximately 75%, are shown in Table 4, together with the corresponding mitigation weights. In this case as well, $\ell_{\text{th}} = 0.5$.

The estimated positions and the RMSE for the outdoor LTE scenario are shown in Fig. 16 and 17, respectively. From the results in Fig. 17, it can be observed that, even if our mitigation strategy drastically reduces the RMSE, the localization error still seems significant (on the order of 400 m in the best case). This is probably due to the fact that using only four anchors (eNBs) is not sufficient in LTE scenarios. In this case as well, the only exception is the PSO-TSML algorithm, which works very well also in the absence of NLOS link mitigation. While in IoT scenarios the complexity of PSO-TSML prevents its use, this may be attractive in cellular (4G/5G) scenarios.

As in Section 4.1, we now compare the performance of our scheme with a scenario in which the NLOS identification and mitigation parameters are optimized for each target-anchor communication link. In Fig. 18, the RMSE is shown for the considered outdoor LTE scenario, comparing our "average mitigation" approach with that based on per-link optimized mitigation. In all the cases, the best algorithm, i.e., the one with NLOS correction and outlier removal, is considered. Similarly to what observed in Fig. 12 for the indoor WiFi scenario, considering per-link mitigation improves the performance, especially when PI is used.

In order to investigate the impact of LOS/NLOS links, we investigate the performance in other scenarios summarized in Table 2 (with reference to Fig. 7). In Fig. 19, we directly compare the performance in all LTE virtual scenarios. One should note that, unlike scenario 1

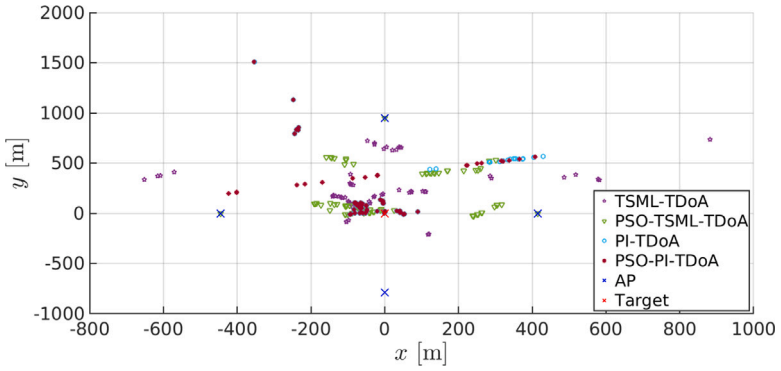

Fig. 16. Estimated positions in the outdoor LTE scenario 1 (see Fig. 7 and Table 2) with outlier removal.

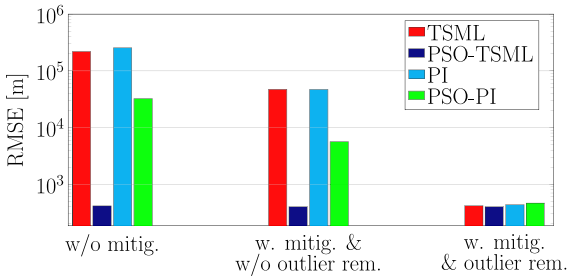

Fig. 17. RMSE for the outdoor LTE scenario 1 (see Fig. 7 and Table 2).

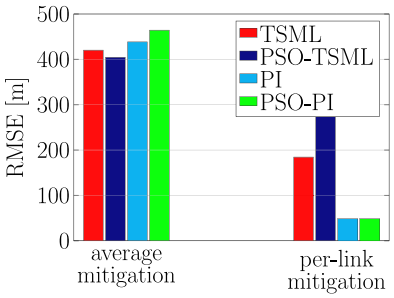

Fig. 18. RMSE for the considered outdoor LTE-based scenario 1 (see Fig. 7 and Table 2), comparing our "average mitigation" approach with an approach based on per-link optimized mitigation.

where all the algorithms achieve approximately the same performance, in other cases the TSML algorithm guarantees the lowest position error. Moreover, the PI has the worst performance approximately in all scenarios.

4.3. Indoor/outdoor scenario comparison

We finally compare directly the performance of the proposed localization method, with NLOS pre-mitigation, in the considered outdoor (LTE) and indoor (WiFi) scenarios. In Fig. 20, the ROC curves for the outdoor LTE scenario 1 (see Fig. 7 and Table 2) and indoor WiFi scenario 1 (see Fig. 5 and Table 1) are directly compared, considering both the reference NN and the best (weighed) classifier. One can observe that the reference NN classifier has approximately the same performance in indoor and outdoor scenarios. On the other hand, the weighed classifier has better performance in the indoor case. The shapes of the ROC curves with the weighed classifier are the same in indoor and outdoor scenarios.

We now set to compare the localization accuracy in outdoor LTE scenario 1 (see Fig. 7 and Table 2) and indoor WiFi scenario 1 (see Fig. 5 and Table 1). In order to make a fair comparison, we "normalize" the RMSE with respect to the average distance between target and anchors, which is 650 m in the outdoor scenario and approximately 8.62 m in the indoor scenario. Therefore, the normalized RMSE is a relative measure of the localization estimation error with respect to the considered topology. In Fig. 21, we compare the normalized RMSEs in outdoor LTE (from Fig. 17) and indoor WiFi (from Fig. 11) scenarios: in all cases, NLOS pre-mitigation, together with outlier removal, is considered. It is worth noting that, except for the PSO-TSML, the relative RMSE is approximately the same for all considered algorithms in both scenarios. This is a desirable feature of the proposed strategy, since it means that its performance is not affected by the specific scenario. Intuitively, this can be justified by the fact that communication bandwidths are similar in outdoor and indoor scenarios and it is well-known that the localization error is approximately inversely proportional to such a quantity [38]. A thorough analytical demonstration of this behavior is the subject of on-going research.

5. Concluding remarks

In this paper, we have investigated a pragmatic approach to RSSI-based localization. This is attractive in scenarios where positioning is performed by (resource-constrained) IoT COTS devices. In order to limit the computational complexity, the key idea is to perform channel status identification (LOS/NLOS), in order to mitigate the identified NLOS links before carrying out localization. In particular, identification and mitigation are based on the computation of significant statistical features over observation windows of N consecutive RSSI samples. Our results show that high channel status identification accuracy can be achieved by simply using a threshold detector based on a single statistical feature of the RSSI, namely the PP. Mitigation has then been performed by deriving a single average correction coefficient for the distance estimates associated with NLOS links, in order to transform them into equivalent LOS links. The use of a single average correction coefficient significantly limits the computational complexity of the mitigation phase. The performance can be significantly improved considering per link optimized identification and mitigation, at the cost of a much higher computational complexity.

A few state-of-the-art localization algorithms have then been considered and experimental performance assessment has been carried out in indoor (WiFi) and outdoor (LTE) scenarios. Our results show that (low-complexity) localization algorithms (namely, TSML and PI) significantly benefit, in terms of position error reduction, from the use of NLOS mitigation. In general, TSML-PSO guarantees the best performance in all considered scenarios, regardless of NLOS link mitigation. In indoor (WiFi-based) and outdoor (LTE-based) scenarios, with average NLOS mitigation (applied to any target-anchor NLOS link), the lowest RMSEs are around 30% and 60% of the average target-anchor distance, respectively. When NLOS mitigation is performed on a per-link basis, the PI algorithm can achieve a RMSE, normalized to the average target-anchor distance, on the order of 10% in both indoor

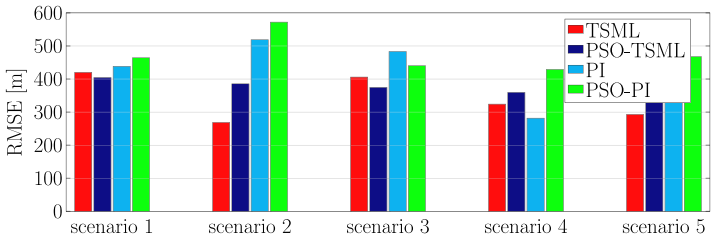

Fig. 19. RMSE results for the outdoor LTE scenarios introduced in Fig. 7 and Table 2.

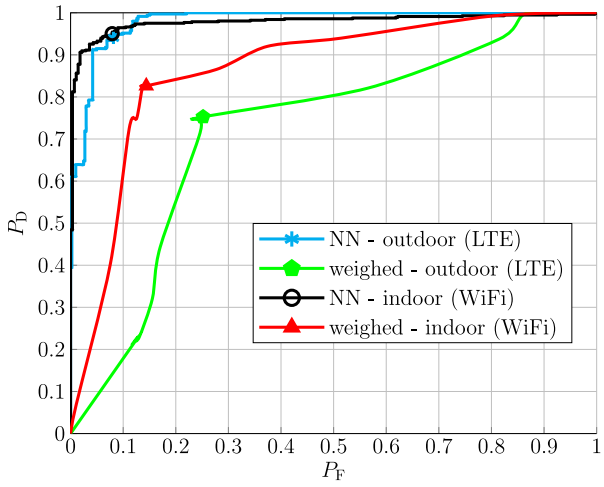

Fig. 20. Comparison of the ROC curves for the outdoor LTE scenario 1 (see Fig. 7 and Table 2) and indoor WiFi scenario 1 (see Fig. 5 and Table 1), considering both the reference NN and the best (weighed) classifier.

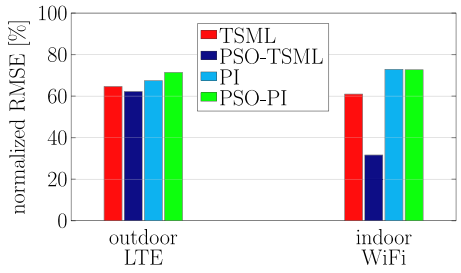

Fig. 21. Comparison of the normalized RMSE for the outdoor LTE scenario 1 (see Fig. 7 and Table 2) and indoor WiFi scenario 1 (see Fig. 5 and Table 1).

WiFi and outdoor LTE scenarios. The performance of our approach in indoor WiFi scenarios compares favorably with that of an approach which relies of UWB RSSI.

CRediT authorship contribution statement

Fabrizio Carpi: Conceptualization, Investigation, Software, Writing – reviewing & editing. **Marco Martalò:** Conceptualization, Investigation, Writing – reviewing & editing. **Luca Davoli:** Conceptualization, Investigation, Writing – reviewing & editing. **Antonio Cilfone:** Conceptualization, Investigation, Software. **Yingjie Yu:** Conceptualization, Methodology, Supervision. **Yi Wang:** Conceptualization, Methodology, Supervision. **Gianluigi Ferrari:** Conceptualization, Methodology, Supervision, Writing – reviewing & editing.

Declaration of competing interest

The authors declare that they have no known competing financial interests or personal relationships that could have appeared to influence the work reported in this paper.

Data availability

The authors are unable or have chosen not to specify which data has been used.

Acknowledgment

This work was supported by the Huawei Innovation Research Program (HIRP) under Grant No. 0892.

References

[1] J.A. del Peral-Rosado, R. Raulefs, J.A. López-Salcedo, G. Seco-Granados, Survey of cellular mobile radio localization methods: From 1G to 5G, IEEE Commun. Surv. Tutor. 20 (2) (2018) 1124–1148, http://dx.doi.org/10.1109/COMST.2017.2785181.

[2] Y. Li, Y. Zhuang, X. Hu, Z. Gao, J. Hu, L. Chen, Z. He, L. Pei, K. Chen, M. Wang, X. Niu, R. Chen, J. Thompson, F. Ghannouchi, N. El-Sheimy, Toward location-enabled IoT (LE-IoT): IoT positioning techniques, error sources, and error mitigation, IEEE Internet Things J. 8 (6) (2021) 4035–4062, http://dx.doi.org/10.1109/JIOT.2020.3019199.

[3] F. Zafari, A. Gkelias, K. Leung, A survey of indoor localization systems and technologies, IEEE Commun. Surveys Tutor. 21 (3) (2019) 2568–2599, http://dx.doi.org/10.1109/COMST.2019.2911558.

[4] Y. Zhao, Z. Zhang, T. Feng, W. Wong, H.K. Garg, GraphIPS: Calibration-free and map-free indoor positioning using smartphone crowdsourced data, IEEE Internet Things J. 8 (1) (2021) 393–406, http://dx.doi.org/10.1109/JIOT.2020.3004703.

[5] S. Sadowski, P. Spachos, K.N. Plataniotis, Memoryless techniques and wireless technologies for indoor localization with the Internet of Things, IEEE Internet Things J. 7 (11) (2020) 10996–11005, http://dx.doi.org/10.1109/JIOT.2020.2992651.

[6] L. Chen, I. Ahriz, D. Le Ruyet, AoA-aware probabilistic indoor location fingerprinting using channel state information, IEEE Internet Things J. 7 (11) (2020) 10868–10883, http://dx.doi.org/10.1109/JIOT.2020.2990314.

[7] Y. Li, X. Hu, Y. Zhuang, Z. Gao, P. Zhang, N. El-Sheimy, Deep reinforcement learning (DRL): Another perspective for unsupervised wireless localization, IEEE Internet Things J. 7 (7) (2020) 6279–6287, http://dx.doi.org/10.1109/JIOT.2019.2957778.

[8] J. Talvitie, M. Renfors, M. Valkama, E.S. Lohan, Method and analysis of spectrally compressed radio images for mobile-centric indoor localization, IEEE Trans. Mob. Comput. 17 (4) (2018) 845–858, http://dx.doi.org/10.1109/TMC.2017.2741487.

[9] Z. Kasmi, N. Guerchali, A. Norrdine, J.H. Schiller, Algorithms and position optimization for a decentralized localization platform based on resource-constrained devices, IEEE Trans. Mob. Comput. 18 (8) (2019) 1731–1744, http://dx.doi.org/10.1109/TMC.2018.2868930.

[10] S. Kumar, S.K. Das, Target detection and localization methods using compartmental model for Internet of Things, IEEE Trans. Mob. Comput. 19 (9) (2020) 2234–2249, http://dx.doi.org/10.1109/TMC.2019.2921537.

[11] S. Shao, A. Khreishah, I. Khalil, Enabling real-time indoor tracking of IoT devices through visible light retroreflection, IEEE Trans. Mob. Comput. 19 (4) (2020) 836–851, http://dx.doi.org/10.1109/TMC.2019.2901665.

[12] F. Shahzad, T.R. Sheltami, E.M. Shakshuki, DV-maxHop: A fast and accurate range-free localization algorithm for anisotropic wireless networks, IEEE Trans. Mob. Comput. 16 (9) (2017) 2494–2505, http://dx.doi.org/10.1109/TMC.2016.2632720.

[13] Y. Zhao, X. Li, Y. Ji, C. Xu, Wireless power-driven positioning system: Fundamental analysis and resource allocation, IEEE Internet Things J. 6 (6) (2019) 10421–10430, http://dx.doi.org/10.1109/JIOT.2019.2939215.

[14] Z. Shi, Y. Wang, User positioning by exploring MIMO measurements with particle swarm optimization, in: Proc. IEEE Intern. Symp. on Personal, Indoor, and Mobile Radio Commun., PIMRC, Montreal, Canada, 2017, pp. 1–5, http://dx.doi.org/10.1109/PIMRC.2017.8292644.

[15] F. Carpi, L. Davoli, M. Martalò, A. Cilfone, Y. Yu, Y. Wang, G. Ferrari, RSSI-based methods for LOS/NLOS channel identification in indoor scenarios, in: Proc. Int. Symp. Wireless Communication Systems, ISWCS, Oulu, Finland, 2019, pp. 171–175, http://dx.doi.org/10.1109/ISWCS.2019.8877315.

[16] J. Choi, W. Lee, J. Lee, J. Lee, S. Kim, Deep learning based NLOS identification with commodity WLAN devices, IEEE Trans. Veh. Technol. 67 (4) (2018) 3295–3303, http://dx.doi.org/10.1109/TVT.2017.2780121.
[17] C. Jiang, J. Shen, S. Chen, Y. Chen, D. Liu, Y. Bo, UWB NLOS/LOS classification using deep learning method, IEEE Commun. Lett. 24 (10) (2020) 2226–2230, http://dx.doi.org/10.1109/LCOMM.2020.2999904.
[18] S. Zhang, C. Yang, D. Jiang, X. Kui, S. Guo, A.Y. Zomaya, J. Wang, Nothing blocks me: Precise and real-time LOS/NLOS path recognition in RFID systems, IEEE Internet Things J. 6 (3) (2019) 5814–5824, http://dx.doi.org/10.1109/JIOT.2019.2907555.
[19] S. Maranò, W.M. Gifford, H. Wymeersch, M.Z. Win, NLOS identification and mitigation for localization based on UWB experimental data, IEEE J. Select. Areas Commun. 28 (7) (2010) 1026–1035, http://dx.doi.org/10.1109/JSAC.2010.100907.
[20] Y. Chen, S. Huang, T. Wu, W. Tsai, C. Liou, S. Mao, UWB system for indoor positioning and tracking with arbitrary target orientation, optimal anchor location, and adaptive NLOS mitigation, IEEE Trans. Veh. Technol. 69 (9) (2020) 9304–9314, http://dx.doi.org/10.1109/TVT.2020.2972578.
[21] S. Tomic, M. Beko, A bisection-based approach for exact target localization in NLOS environments, Elsevier Signal Process. 143 (2018) 328–335, http://dx.doi.org/10.1016/j.sigpro.2017.09.019.
[22] S. Tomic, M. Beko, A robust NLOS bias mitigation technique for RSS-TOA-based target localization, IEEE Signal Process. Lett. 26 (1) (2019) 64–68, http://dx.doi.org/10.1109/LSP.2018.2879720.
[23] G. Wang, W. Zhu, N. Ansari, Robust TDOA-based localization for IoT via joint source position and NLOS error estimation, IEEE Internet Things J. 6 (5) (2019) 8529–8541, http://dx.doi.org/10.1109/JIOT.2019.2920081.
[24] X. Cai, X. Li, R. Yuan, Y. Hei, Identification and mitigation of NLOS based on channel state information for indoor WiFi localization, in: Proc. Int. Conf. Wireless Communications Signal Processing, WCSP, Nanjing, China, 2015, pp. 1–5, http://dx.doi.org/10.1109/WCSP.2015.7341172.
[25] K. Bregar, M. Mohorčič, Improving indoor localization using convolutional neural networks on computationally restricted devices, IEEE Access 6 (2018) 17429–17441, http://dx.doi.org/10.1109/ACCESS.2018.2817800.
[26] M. Katwe, P. Ghare, P.K. Sharma, A. Kothari, NLOS error mitigation in hybrid RSS-TOA based localization through semi-definite relaxation, IEEE Commun. Lett. 24 (12) (2020) 2761–2765, http://dx.doi.org/10.1109/LCOMM.2020.3020948.
[27] Y. Wang, K. Gu, Y. Wu, W. Dai, Y. Shen, NLOS effect mitigation via spatial geometry exploitation in cooperative localization, IEEE Trans. Wirel. Commun. 19 (9) (2020) 6037–6049, http://dx.doi.org/10.1109/TWC.2020.2999667.
[28] A. Goldsmith, Wireless Communications, Cambridge University Press, New York, NY, USA, 2005.
[29] Y. Chan, K.C. Ho, A simple and efficient estimator for hyperbolic location, IEEE Trans. Signal Process. 42 (8) (1994) 1905—1915, http://dx.doi.org/10.1109/78.301830.
[30] R.O. Schmidt, A new approach to geometry of range difference location, IEEE Trans. Aerosp. Electron. Syst. AES-8 (6) (1972) 821–835, http://dx.doi.org/10.1109/TAES.1972.309614.
[31] K. Cengiz, Comprehensive analysis on least squares lateration for indoor positioning systems, IEEE Internet Things J. 8 (4) (2021) 2842–2856, http://dx.doi.org/10.1109/JIOT.2020.3020888.
[32] S. Bottigliero, D. Milanesio, M. Saccani, R. Maggiora, A low-cost indoor real-time locating system based on TDOA estimation of UWB pulse sequences, IEEE Trans. Instrum. Meas. 70 (2021) 1–11, http://dx.doi.org/10.1109/TIM.2021.3069486.
[33] Å. Björck, Linear Algebra and Its Applications, Elsevier Science Publishers, 1987.
[34] H. Cui, Y. Liang, C. Zhou, N. Cao, Localization of large-scale wireless sensor networks using Niching particle swarm optimization and reliable anchor selection, Hindawi Wirel. Commun. Mob. Comput. (2018) 2473875, http://dx.doi.org/10.1155/2018/2473875.
[35] S. Monica, G. Ferrari, Swarm intelligent approaches to auto-localization of nodes in static UWB networks, Appl. Soft Comput. 25 (2014) 426–434, http://dx.doi.org/10.1016/j.asoc.2014.07.025.
[36] S. Monica, G. Ferrari, Maximum likelihood localization: When does it fail? ICT Express 2 (1) (2016) 10–13, http://dx.doi.org/10.1016/j.icte.2016.02.004.
[37] J. Kennedy, R. Eberhart, Particle swarm optimization, in: Proc. Int. Conf. Neural Networks, Vol. 4, ICNN, Perth, WA, Australia, 1995, pp. 1942–1948, http://dx.doi.org/10.1109/ICNN.1995.488968.
[38] S. Gezici, Z. Tian, G.B. Giannakis, H. Kobayashi, A.F. Molisch, H.V. Poor, Z. Sahinoglu, Localization via ultra-wideband radios: A look at positioning aspects for future sensor networks, IEEE Signal Process. Mag. 22 (4) (2005) 70–84, http://dx.doi.org/10.1109/MSP.2005.1458289.

Fabrizio Carpi received his M.Sc. degree in Communication Engineering from University of Parma, Italy, in 2018. He is currently a Ph.D. candidate in Electrical Engineering at New York University Tandon School of Engineering. He is also a member of NYU WIRELESS Center conducting research on next-generation wireless networks. His research interests include wireless communications, source and channel coding, information theory, and machine learning.

Marco Martalò received the Ph.D. in Information Technologies from the University of Parma, Italy, in 2009. From 2012 to 2017, he was an Assistant Professor with E-Campus University, Italy, and also a Research Associate with the University of Parma, Italy, until 2020. Since 2020, he is an Associate Professor of Telecommunications at the University of Cagliari, Italy, where he is part of the Networks for Humans (Net4U) laboratory. He has co-authored the book "Sensor Networks with IEEE 802.15.4 Systems: Distributed Processing, MAC, and Connectivity." His research interests are in the design of communication and signal processing algorithms for wireless systems and networks, as well as security aspects to them. He is an IEEE Senior Member.

Luca Davoli is currently a Fixed-term Assistant Professor at the Department of Engineering and Architecture of the University of Parma. He received his Ph.D. in Information Technologies in 2017 and, since January 2014, he has been a member of the Internet of Things (IoT) Laboratory at the same university. He has (published or in press) over 35 papers, and has been TPC member of international conferences and served on the editorial boards and as Guest Editor of international journals. His main research interests are in the fields of Internet of Things, Software Defined Networking, Big Stream and Peer-to-Peer Networks.

Antonio Cilfone received his Master of Science in Communication Engineering and his Ph.D. in Information Technologies from the University of Parma, Parma, Italy, in 2016 and 2019, respectively. He has been member of the Internet of Things (IoT) Lab at the Department of Engineering and Architecture of the University of Parma from 2016 until 2020, working in heterogeneous networking, signal processing and smart systems fields. He is currently working as R&D software engineer for Tesmec Automation S.r.l., Italy.

Yingjie Yu received the B.S., M.S., and Ph.D. degrees in communication and information system from Northwestern Polytechnical University, Xi'an, China, in 2011, 2014, and 2018, respectively. She is currently a senior engineer in Huawei Technologies Co.,Ltd working on 5G positioning research.

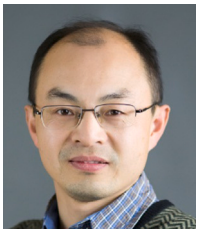

Dr. Yi Wang is currently a principal engineer at Huawei Technologies Co., Ltd. in Shanghai. Since 2005 he joined Huawei Technologies Co., Ltd. he led a series of research projects on LTE/LTE-Advanced and 5G. Currently he is leading 5G positioning research in Huawei. Dr. Yi Wang owns granted 150+ patents and 90+ papers. Many patents have been realized in LTE/LTE-Advanced and 5G products and adopted in 3GPP and IEEE802.11 standards. Dr. Yi Wang is the board member of NYU Wireless Industrial Affiliates since 2014. He is the chair of China IMT-2020 (5G) mmWave Technology since 2013.

Gianluigi Ferrari is a Full Professor of Telecommunications at the University of Parma, Italy, where he received his PhD in Information Technologies in 2002. Since September 2006 he has been the Coordinator of the Internet of Things (IoT) Laboratory (http://iotlab.unipr.it/) and, since 2016, he has been the co-founder and President of things2i s.r.l. (http://www.things2i.com/), a spin-off company of the University of Parma dedicated to IoT and smart systems. His research activities revolve around signal processing, communication/networking, and IoT. He has published and consulted extensively in these areas, coordinating several technical projects, including EU-funded competitive projects. He is currently the Head of the Bachelor Degree in Computer Engineering, Electronics and Telecommunications of the University of Parma (https://cdl-iiet.unipr.it/) and a member of the Scientific Council of the INSIDE Industry Association (https://www.inside-association.eu/). He is an IEEE Senior Member.